Charge-Transfer States and Antiferromagnetism of Bridged Cu Dimers: Application to Oxyhemocyanin

Felix Tuczek† and Edward I. Solomon*

Contribution from the Department of Chemistry, Stanford University, Stanford, California 94305

Received January 7, 1994®

Abstract: New low-energy intense bands are observed in the electronic absorption spectra of binuclear bridged transition-metal dimers which are not present in the spectra of the corresponding mononuclear compounds. These features are assigned as singlet charge-transfer transitions greatly lowered in energy due to large charge-transfer excited-state antiferromagnetic coupling. In addition, monomer charge-transfer transitions can split in energy in a dimer, and this splitting is experimentally observed to be much larger than that given by the interaction between charge-transfer transitions to the two coppers of the dimer. A valence bond configuration interaction model is presented which is applied to the peroxide → Cu(II) charge-transfer spectrum of oxyhemocyanin and to the charge-transfer spectrum of a binuclear copper peroxide model complex with the side-on bridging (μ-η^2:η^2) structure. This model accounts for both the excited-state antiferromagnetism and the energy splitting of the peroxide → Cu charge-transfer transitions in the dimer. The observed charge-transfer excited-state spectral features provide insight into the bonding of the bridging ligand to the two metal centers. This bridging ligand is responsible for ground-state antiferromagnetic coupling between the metal centers, and thus the charge-transfer transitions of the bridging ligand provide a direct probe of the superexchange pathway in bridged metal dimers.

I. Introduction

Electronic absorption spectra of bridged binuclear metal complexes often show new intense bands in the region between the ligand field (LF) and charge-transfer (CT) transitions which are absent in the spectra of the corresponding mononuclear metal complexes.[1,2] Originally, these "dimer bands" have been attributed to LF transitions occurring simultaneously on both metal centers of the dimer at twice the monomer transition energy (simultaneous pair excitation, SPE).[3] However, the dimer band in the binuclear Cu(II) system $Cu_2Cl_6^{2-}$ has been shown to be a singlet ligand-to-metal charge-transfer transition.[4] The shift to low energy was attributed to a large singlet–triplet splitting in the CT excited state with the singlet at lower energy. This is similar to the behavior observed in the ground state (GS) of copper dimers, where the two $S = {}^1/_2$ centers antiferromagnetically couple to form total spin states of 1 and 0 in the dimer, with $S_{tot} = 0$ below $S_{tot} = 1$ by $-2J^{GS}$ (J is the exchange constant). The antiferromagnetic interaction in the CT excited state was found to be much larger than that in the ground state which derives from the very large, direct overlap between a singly occupied ligand orbital on one half of the dimer and the highest energy, singly occupied copper d orbital on the other half of the dimer.

In addition to a shift to lower energy, electronic spectra further show evidence for the energy splitting of a monomer CT transition into two transitions in the dimer. Thus, the azide $(\pi^{nb})_\sigma$ → Cu CT transition, which is observed at 25 500 cm^{-1} in the monomeric copper(II) azide complex [Cu(L′–O)(N_3)], splits into two transitions at 27 400 and 23 800 cm^{-1} in the *cis*-μ-1,3-azide-bridged Cu(II) dimer $[Cu_2(L\text{-}Et)(N_3^-)]^{2+}$.[5] A transition dipole vector coupling (TDVC) model has been developed to account for the selection rules, intensities, and splittings observed experimentally.[6] Whereas the predictions of the model are qualitatively in agreement with the observations, the calculated value of the energy splitting is an order of magnitude too small.

In this study, a valence bond configuration interaction (VBCI) model is presented which quantitatively explains both the CT state energy splitting and CT excited-state antiferromagnetism in bridged transition-metal dimers. The valence bond (VB) formalism starts from a localized ground-state description of the two $S = {}^1/_2$ Cu(II) centers and introduces a limited amount of delocalization between the coppers through configuration interation (CI) with the metal → metal CT (MMCT) state.[7] This procedure is related to the Anderson theory for ground-state antiferromagnetism.[8] However, LMCT states are not considered in Anderson theory, whereas the VBCI model explicitly includes ligand → Cu CT states in the CI scheme which leads to the observed splitting and antiferromagnetism in these excited states. In addition, Anderson theory explains GS antiferromagnetism by direct configuration interaction between the ground and MMCT states. In this VBCI model, GS antiferromagnetism derives from CI between the GS and the LMCT states, which are subject to large CT excited-state antiferromagnetism. Hence, the VBCI model also provides physical insight into how the energies of CT transitions relate to ground-state properties of dimers: CT transitions provide a direct probe of individual superexchange pathways contributing to the ground-state exchange coupling constant $-2J^{GS}$.

The VBCI model is applied to oxyhemocyanin (oxyHc), which is a binuclear copper protein present in mollusks and arthropods

* Author to whom correspondence should be addressed.
† Present address: Institut für Anorganische und Analytische Chemie, Johannes Gutenberg Universität Mainz, D-55099 Mainz, FRG.
® Abstract published in *Advance ACS Abstracts,* July 1, 1994.

(1) Lever, A. B. P. *Inorganic Electronic Spectroscopy*; Elsevier: New York, 1984.
(2) (a) Dubicki, L. *Aust. J. Chem.* **1972**, *25*, 1141–1149. (b) Hansen, A. E.; Ballhausen, C. J. *Trans. Faraday Soc.* **1965**, *65*, 631. (c) Schugar, H. J.; Rossman, G. R.; Barraclough, C. G.; Gray, H. B. *J. Am. Chem. Soc.* **1972**, *94*, 2683–2690. (d) Schugar, H. J.; Rossman, G. R.; Thibeault, J.; Gray, H. B. *Chem. Phys. Lett.* **1970**, *6*, 26.
(3) (a) McClure, D. S. *J. Chem. Phys.* **1963**, *39*, 2850–2855. (b) Lohr, L. L.; McClure, D. S. *J. Chem. Phys.* **1968**, *49*, 3516–3521. (c) Ferguson, J.; Guggenheim, H. J.; Tanabe, Y. *J. Phys. Soc. Jpn.* **1966**, *21*, 692–704. (d) Decurtins, S.; Güdel, H. U. *Inorg. Chem.* **1982**, *21*, 3598–3606 and references therein.
(4) Desjardins, S. R.; Wilcox, D. E.; Musselman, R. L.; Solomon, E. I. *Inorg. Chem.* **1987**, *26*, 288–300.
(5) Pate, J. E.; Ross, P. K.; Thamann, T. J.; Reed, C. A.; Karlin, K. D.; Sorrell, T. N.; Solomon, E. I. *J. Am. Chem. Soc.* **1989**, *111*, 5198–5208. The ligand L-Et is the anion of *N,N,N′,N′*-tetrakis[2-(1-ethylbenzimidazolyl)]-2-hydroxy-1,3-diaminopropane. McKee, V.; Zvagulis, M.; Dagdigian, J. V.; Patch, M. G.; Reed, C. A. *J. Am. Chem. Soc.* **1984**, *106*, 4765–4772.
(6) Eickman, N. C.; Himmelwright, R. S.; Solomon, E. I. *Proc. Natl. Acad. Sci. U.S.A.* **1979**, *76*, 2094–2098.
(7) Tuczek, F.; Solomon, E. I. *Inorg. Chem.* **1993**, *32*, 2850–2862.
(8) (a) Anderson, P. W. *Phys. Rev.* **1959**, *115*, 2. (b) Anderson, P. W. *Solid State Phys.* **1963**, *14*, 99–214.

0002-7863/94/1516-6916$04.50/0

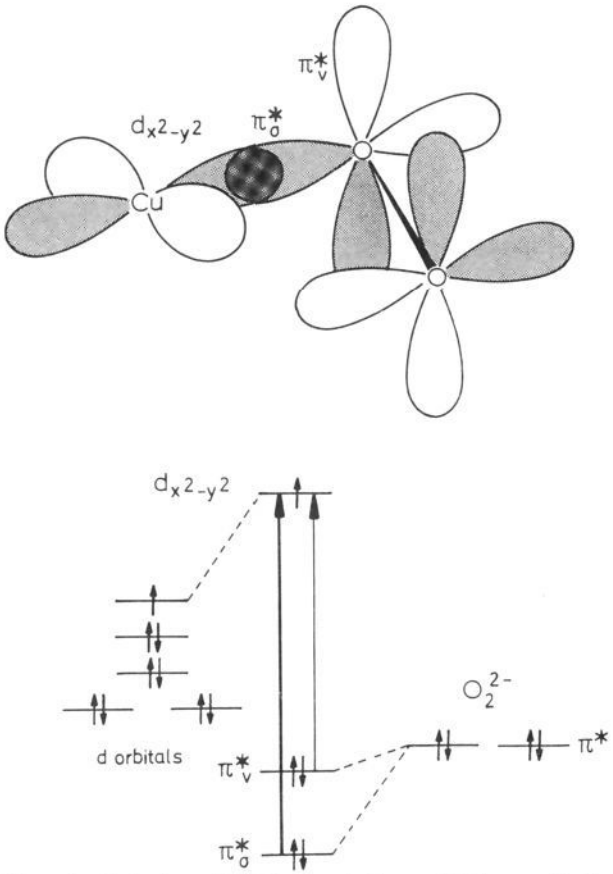

Figure 1. Molecular orbital diagram (valence orbitals on top) of a monomeric copper peroxo complex. The two possible charge-transfer transitions are indicated, with their relative intensities given by the thickness of the arrow.

and generated by the reversible binding of dioxygen.[9] From the crystal structure of the protein[10] and the spectral comparison with a small-molecule analog with the ligand tris(3,5-diisopropylpyrazolyl)borate, $[Cu(HB(3,5\text{-}iPr_2pz)_3]_2(O_2)$,[11] the O_2 is bound as peroxide in a side-on bridging (μ-η^2:η^2) fashion to the copper(II) ions coordinated by histidine nitrogens in a square-pyramidal structure. The ground state is strongly antiferromagnetically coupled through the peroxide bridge ($-2J^{GS} \geq 600$ cm^{-1}).[12] The CT spectra of oxyHc[9] and the side-on bridged model complex[11] are extremely unusual compared to those of all other peroxy Cu(II) complexes and show intense absorption bands at 350 (ϵ = 20 000 M^{-1} cm^{-1}) and 580 nm (ϵ = 1000 M^{-1} cm^{-1}) and a feature in the circular dichroism (CD) spectrum at 480 nm ($\Delta\epsilon$ = +2.5 M^{-1} cm^{-1}) which has no corresponding feature in the absorption spectrum. These are all assigned to $O_2^{2-} \rightarrow$ Cu CT transitions. Peroxide has a doubly degenerate π^* set of valence orbitals which split in energy upon binding to a copper center into an in-plane, σ-bonding orbital, π^*_σ, and an out-of-plane, π-bonding orbital, π^*_v (Figure 1). Hence, two CT transitions are predicted from peroxide to the highest energy, singly occupied $d_{x^2-y^2}$ orbital of a single copper(II) center: a high-energy, high-intensity $\pi^*_\sigma \rightarrow$ Cu(II) and a lower energy, low-intensity $\pi^*_v \rightarrow$ Cu(II) CT

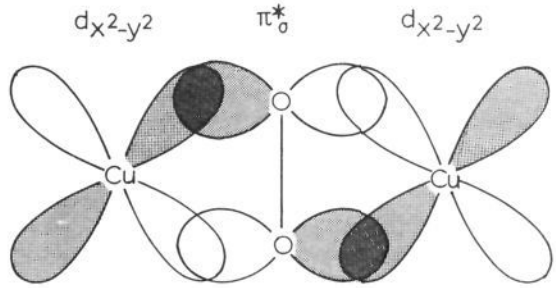

Figure 2. π^*_σ–$d_{x^2-y^2}$ bonding diagram of a side-on (μ-η^2:η^2) peroxide-bridged copper dimer.

transition. The fact that *three* peroxide $\rightarrow$ Cu CT transitions are observed in oxyHc indicates that at least one of the CT transitions has been split by dimer interactions into two states at different energies. The electronic structure of oxyHc has been recently described on the basis of broken-symmetry SCF-Xα-SW calculations, and the CT transition energies have been calculated.[13] The Xα method allows one to estimate excited (e.g., CT)-state energies using the transition-state method.[14] However, due to the broken-symmetry formalism,[15] the splitting in the CT excited states could not be evalulated with these calculations. Whereas the $\pi^*_v \rightarrow$ Cu(II) CT energy obtained with the broken-symmetry Xα transition-state calculations was in good agreement with the experimental data, the $\pi^*_\sigma \rightarrow$ Cu(II) CT energy was much too high. From the above discussion, this discrepancy should be due to the presence of a large excited-state antiferromagnetism in the $\pi^*_\sigma \rightarrow$ Cu CT state which is not accounted for in the molecular orbital calculation. In this study, the VBCI model is employed to analyze the CT spectrum of oxyHc. Using the results of this model, variations in the CT spectra of mollusk and arthropod hemocyanins are further correlated to the experimentally observed differences in the stabilities and reactivities of their binuclear cupric active sites.[16] Finally, the CT spectral features are related to the superexchange pathway leading to the observed ground-state antiferromagnetism of oxyhemocyanin.

II. Valence Bond Configuration Interaction Model

We consider a dimeric Cu(II) complex bridged by peroxide (O_2^{2-}) in a side-on (μ-η^2:η^2) fashion (Figure 2). Only the highest energy orbitals of peroxide, π^*_σ and π^*_v, and the highest energy, singly occupied $d_{x^2-y^2}$ orbitals d_A and d_B of the two Cu centers Cu_A and Cu_B are included in the treatment. It is assumed that in the electronic ground state, each unpaired electron is primarily localized on one copper center. Therefore, a valence bond (VB) formalism is employed. In this description, a ligand $\rightarrow$ metal CT (LMCT) transition corresponds to the transfer of an electron from the π^*_σ or π^*_v orbital of the bridging peroxide to the $d_{x^2-y^2}$ orbital on Cu_A, d_A, or on Cu_B, d_B. Hence, both the $\pi^*_\sigma \rightarrow$ Cu and the $\pi^*_v \rightarrow$ Cu CT states are doubly degenerate in a dimer. However, this degeneracy is lifted by electronic interactions, and two states of *g* and *u* symmetry result for both the $\pi^*_\sigma \rightarrow$ Cu(II) and the $\pi^*_v \rightarrow$ Cu(II) CT transition. These correspond to the symmetric and antisymmetric combinations of the CT transitions to each copper in the dimer. It has been observed that in peroxide[10] and azide-bridged[5] copper dimers, this *g*,*u* energy splitting may

(9) (a) Solomon, E. I.; Baldwin, M. J.; Lowery, M. D. *Chem. Rev.* **1992**, *92*, 521–542. (b) Solomon, E. I. In *Metal Clusters in Proteins*; Que, L., Ed.; ACS Symposium Series 372; American Chemical Society: Washington, DC, 1988; pp 116–150.

(10) Ton-That, H.; Magnus, K. A. *J. Inorg. Biochem.* **1993**, *51*, 65.

(11) Baldwin, M. J.; Root, D. E.; Pate, J. E.; Fujisawa, K.; Kitajima, N.; Solomon, E. I. *J. Am. Chem. Soc.* **1992**, *114*, 10421–10431.

(12) (a) Solomon, E. I.; Dooley, D. M.; Wang, R.-H.; Gray, H. B.; Cerdonio, M.; Mogno, F.; Romani, G. L. *J. Am. Chem. Soc.* **1976**, *98*, 1029–1031. (b) Dooley, D. M.; Scott, R. A.; Ellinghaus, J.; Solomon, E. I.; Gray, H. B. *Proc. Natl. Acad. Sci. U.S.A.* **1978**, *75*, 3019–3022.

(13) (a) Ross, P. K.; Solomon, E. I. *J. Am. Chem. Soc.* **1990**, *112*, 5871–5872. (b) Ross, P. K.; Solomon, E. I. *J. Am. Chem. Soc.* **1991**, *113*, 3246–3259.

(14) (a) Slater, J. C. *The Self-consistent Field for Molecules and Solids*; Mc-Graw-Hill: New York, 1974; Vol. 4. (b) Johnson, K. H. *Adv. Quantum Chem.* **1973**, *7*, 143–185.

(15) (a) Noodleman, L.; Norman, J. G., Jr. *J. Chem. Phys.* **1979**, *70*, 4903–4906. (b) Noodleman, L. *J. Chem. Phys.* **1981**, *74*, 5737–5743.

(16) Himmelwright, R. S.; Eickman, N. C.; LuBien, C.; Solomon, E. I. *J. Am. Chem. Soc.* **1980**, *102*, 5378–5388.

be on the order of several 1000 cm^{-1}. Further, each localized LMCT transition changes the configuration on one copper(II) from d^9 to d^{10} (closed shell) and leaves an unpaired electron in the respective ligand orbital (π^*_σ or π^*_v). Spin coupling of this electron with the unpaired electron in the d orbital on the other copper generates CT singlet and CT triplet states. The corresponding singlet–triplet splitting has been found to be strongly antiferromagnetic, i.e., the singlets are at much lower energy than the triplets.[4] In this section, a VB description is developed for the CT transitions from the peroxide π^*_σ orbital to the coppers in a side-on peroxide-bridged dimer. It is shown how configuration interaction (CI) between the LMCT states and the ground and higher energy CT states influences the energies and splittings of the LMCT states as well as the magnetic properties of the electronic ground state. This VBCI model is related to cluster-CI methods of solid-state theory.[17] In section III, the VBCI model is applied to the $\pi^*_\sigma \rightarrow$ Cu CT transition in oxyhemocyanin (D_{2h} symmetry as in Figure 2) and related to spectroscopic data and the antiferromagnetism of the ground state. It is then extended to consider state splittings in the $\pi^*_v \rightarrow$ Cu CT transition. This differs from the π^*_σ transition in that there is no overlap between the π^*_v orbital and the Cu $d_{x^2-y^2}$ orbitals in D_{2h} symmetry. From the VBCI model presented below, this means that in the D_{2h} limit there can be no contribution of the π^*_v CT excited state to the ground-state coupling constant $-2J^{GS}$.

Within the three-orbital (d_A, d_B, π^*_σ), four-electron (one on each copper and two in π^*_σ) system described above, the ground-state (GS) configuration for a side-on peroxide-bridged Cu(II) dimer (D_{2h} symmetry) is represented by

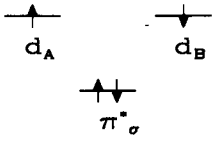

(I)

The resulting singlet and triplet states are $^1A_g^{GS}$ and $^3B_{3u}^{GS}$, where ^1A_g is symmetric and $^3B_{3u}$ antisymmetric with respect to the center of inversion of the dimer. A LMCT configuration generated by a CT transition from π^*_σ to d_A is represented by

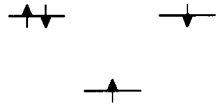

(II)

The CT transition can alternatively involve d_B, which leads to four CT excited singlet and triplet states $^1A_g^{CT}$, $^1B_{3u}^{CT}$, $^3A_g^{CT}$, and $^3B_{3u}^{CT}$, as described above. Neglecting small two-electron matrix elements,[7] these CT states are degenerate at an energy Δ above the ground state. Here, the CT energy Δ is given by the zeroth-order energy difference between the π^*_σ orbital and the d_A (or d_B) orbital on the metal. Ground and CT excited states of the same symmetry interact via the transfer matrix element

$$\langle {}^3B_{3u}{}^{GS}|H|{}^3B_{3u}{}^{CT}\rangle = \langle {}^1A_g{}^{GS}|H|{}^1A_g{}^{CT}\rangle = \sqrt{2}\langle d_A|h|\pi^*_\sigma\rangle \equiv \sqrt{2}h_{d_A\pi} = \sqrt{2}h_{d_B\pi} \equiv h_{d\pi} \quad (1)$$

which depends on the overlap between metal and ligand orbitals and introduces the bonding interaction between the bridging ligand and the metal centers into our description. The Hamiltonian H in (1) is given by a sum of one-electron operators $h(i)$ acting on

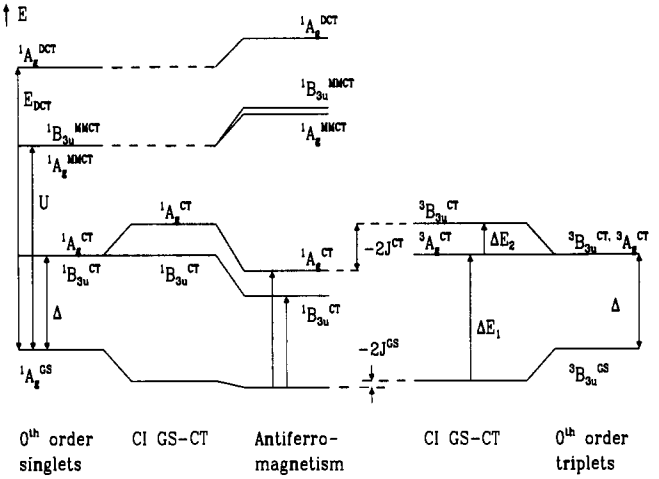

Figure 3. VBCI diagram for a side-on peroxide-bridged copper dimer. Right half, triplet states; left half, singlet states. In the triplets (from right to middle) and in the singlets (from left to middle), configuration interaction is introduced between the GS and CT (singlet, triplets) and the CT and higher energy MMCT and DCT states, respectively (singlets, middle of diagram). The two transition energies ΔE_1 and ΔE_2 are obtained by triplet SCF-Xα transition-state calculations, and the two singlet CT transitions (middle) are obtained by diagonalization of (3) and (4).

electron i and the electron–electron interaction e^2/r_{ij}. Denoting diagonal matrix elements of H by $\langle\Gamma\rangle$ and zeroth-order energies with $\langle {}^3B_{3u}{}^{CT}\rangle - \langle {}^3B_{3u}{}^{GS}\rangle = \Delta$, the triplet secular determinant is given by eq 2:

$$\begin{vmatrix} \langle {}^3B_{3u}{}^{GS}\rangle - E & h_{d\pi} \\ h_{d\pi} & \langle {}^3B_{3u}{}^{CT}\rangle - E \end{vmatrix} = \begin{vmatrix} -E & h_{d\pi} \\ h_{d\pi} & \Delta - E \end{vmatrix} = 0 \quad (2)$$

This describes the mutual repulsion between the triplet ground and $^3B_{3u}{}^{CT}$ CT excited states leading to a mixing between $^3B_{3u}{}^{CT}$ and $^3B_{3u}{}^{GS}$, a stabilization of the admixed triplet ground state $^3B_{3u}{}^{GS}$ by approximately $h_{d\pi}{}^2/\Delta$, and a shift of the admixed $^3B_{3u}{}^{CT}$ triplet CT state above Δ by the same amount (Figure 3, right). Since the symmetric component of the CT excited state $^3A_g{}^{CT}$ cannot interact with the ground state (and, in fact, with no other state in this model), the triplet CT states split into g and u components by $\Delta E_2 \approx h_{d\pi}{}^2/\Delta$, with the u component being at higher energy.

Analogous considerations apply for the singlet ground and CT excited states. Here, the *sym* components $^1A_g{}^{GS}$ and $^1A_g{}^{CT}$ interact, leading to a stabilization of the admixed singlet $^1A_g{}^{GS}$ ground state by approximately $h_{d\pi}{}^2/\Delta$ and a shift of the admixed $^1A_g{}^{CT}$ state above Δ by the same amount. Since $^1B_{3u}{}^{CT}$ does not interact with the ground state, the singlet CT states are split by approximately $h_{d\pi}{}^2/\Delta$, with the g component at higher energy (Figure 3, left). Note that at this point this singlet energy splitting order is opposite that of the triplet CT states on the right of Figure 3 and that the $^1A_g{}^{GS}$ ground state is at the same energy as the triplet $^3B_{3u}{}^{GS}$ state which corresponds to zero magnetic coupling. However, there exist two additional higher energy singlet CT states which can interact with the $^1A_g{}^{CT}$ and $^1B_{3u}{}^{CT}$ LMCT states and the $^1A_g{}^{GS}$ ground state. Starting from the LMCT configuration (II), the unpaired electron on d_B can be transferred to the bridge. By comparison with the GS configuration (I), this corresponds to a metal-to-metal CT (MMCT) state where the unpaired electron on one copper has been transferred to the other copper:

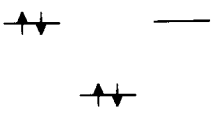

(III)

(17) (a) Zaanen, J.; Sawatzki, G. A. *Can. J. Phys.* **1987**, *65*, 1262–1271. (b) Sawatzki, G. A. *Int. J. Mod. Phys. B* **1988**, *1*, 243–266. (c) Shen, Z.-X.; Allen, J. W.; Yeh, J. J.; Kang, J.-S.; Ellis, W.; Spicer, W.; Lindau, I.; Maple, M. B.; Dalichaouch, Y. D.; Torikachvili, M. S.; Sun, J. Z.; Geballe, T. H. *Phys. Rev. B* **1987**, *36*, 8414–8428.

Further, the unpaired electron in the peroxide orbital of the LMCT excited state (II) can be transferred to d_B, leaving a doubly vacant π^* orbital (double CT, DCT) as in (IV):

(IV)

Whereas the DCT state is of ^1A_g symmetry, the MMCT states have ^1A_g and $^1B_{3u}$ symmetry. This covers all possible states within the three orbital, four electron model in (I–IV). Thus, the two following secular determinants apply for the singlets:

$$\begin{vmatrix} \langle {}^1B_{3u}{}^{CT}\rangle - E & h_{d\pi} \\ h_{d\pi} & \langle {}^1B_{3u}{}^{MMCT}\rangle - E \end{vmatrix} = 0 \qquad (3)$$

$$\begin{vmatrix} \langle {}^1A_g^{GS}\rangle - E & h_{d\pi} & 0 & 0 \\ h_{d\pi} & \langle {}^1A_g^{CT}\rangle - E & h_{d\pi} & \sqrt{2}h_{d\pi} \\ 0 & h_{d\pi} & \langle {}^1A_g^{MMCT}\rangle - E & 0 \\ 0 & \sqrt{2}h_{d\pi} & 0 & \langle {}^1A_g^{DCT}\rangle - E \end{vmatrix} = 0 \qquad (4)$$

The secular determinants 2–4 involve three zeroth-order energies, the LMCT energy $\Delta = \langle \Gamma^{CT}\rangle - \langle \Gamma^{GS}\rangle$, the energy of the MMCT states $U = \langle \Gamma^{MMCT}\rangle - \langle \Gamma^{GS}\rangle$, the energy of the DCT state $E_{DCT} = \langle {}^1A_{1g}{}^{DCT}\rangle - \langle \Gamma^{GS}\rangle$, and a value for the transfer matrix element, $h_{d\pi}$. From photoelectron spectroscopy of bridged copper dimers, the Mott–Hubbard energy U is estimated at 6.5 eV.[18] The remaining parameters are evaluated with the help of SCF-Xα transition-state calculations. To this end, the molecular orbital (MO) description of the peroxo-bridged copper dimer is briefly presented.

In the MO framework, the two highest energy, singly occupied copper $d_{x^2-y^2}$ orbitals d_A and d_B are combined to form the molecular orbitals

$$d_1 \equiv (1/\sqrt{2})(d_A + d_B) \qquad d_2 \equiv (1/\sqrt{2})(d_A - d_B) \quad (5)$$

One combination has the same symmetry as π^* and, therefore, has a bonding antibonding interaction with π^* leading to a shift of this MO above Δ and a stabilization of the π^* orbital (*cf.* Figure 2, both the "g" combination of the $d_{x^2-y^2}$ orbitals and π^*_σ have B_{1g} symmetry in the D_{2h} point group). The symmetry of the other combination (B_{2u}, not displayed) is different from π^*_σ, and there is no interaction. Hence, when d_1 and d_2 split in energy, the lower energy combination (B_{2u}) becomes the HOMO and the higher energy combination (B_{1g}) the LUMO of the binuclear complex, and the splitting between the two MOs becomes the HOMO–LUMO gap ΔE_{HL}.

Based on the restricted set of HOMO, LUMO, and peroxide π^*_σ orbitals, four-electron MO states can be formulated. The LUMO having some π^*_σ character is denoted by LUMO′ and π^* orbital having some metal character by $(\pi^*_\sigma)'$. The MO ground-state configuration is represented by

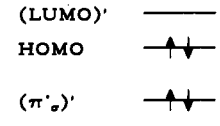

(V)

Note that this configuration differs from the VB counterpart (I) by having two electrons placed in a delocalized molecular orbital and thus represents a poor description of the electronic ground state of copper dimers.[19] In contrast, the MO GS triplet M_S = 1 wave function

(VI)

is identical with that of the VB state and provides a proper description of the triplet ground state.[15,19] In the MO framework, charge-transfer states are generated by moving one electron from $(\pi^*_\sigma)'$ to the HOMO or the LUMO′. For example, triplet M_S = 1 LMCT states are given by (VII) and (VIII):

(VII)

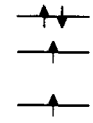

(VIII)

It has been shown previously that, in analogy to the triplet ground state, these triplet MO CT states are identical to their VB counterparts,[7] i.e., (VII) and (VIII) are alternative representations for the VB states $^3A_g{}^{CT}$ and $^3B_{3u}{}^{CT}$ after diagonalization of the triplet CI matrix (2). Hence, the energies of the triplet MO states must be identical to the energies of the VBCI triplet states. The equivalence between the MO and VBCI formalism, however, does not hold for the description of the singlet CT states. This discrepancy is mainly due to a different way in which MO (at the Hartree–Fock level) and VB theories take the "ionic" MMCT configuration into account.

The relative energies of the MO triplet states can be determined with SCF-Xα transition-state calculations. In this method, half an electron is moved from a donor to an acceptor orbital, and, after reconverging the potential, the energy difference between these two orbitals is identified with the electronic transition energy.[14] Thus, the lower energy triplet CT state $^3A_g{}^{CT}$ (VII) is reached from the triplet M_S = 1 ground-state $^3B_{3u}{}^{GS}$ (VI) by a transition of a β electron from $(\pi^*_\sigma)'$ to the HOMO. The corresponding transition-state calculation provides a value for the energy difference

$$\Delta E[{}^3A_g{}^{CT} - {}^3B_{3u}{}^{GS}] \equiv \Delta E_1 \qquad (6)$$

(see Figure 3). Likewise, the energy difference between the two triplet CT states

$$\Delta E[{}^3B_{3u}{}^{CT} - {}^3A_g{}^{CT}] \equiv \Delta E_2 \qquad (7)$$

is determined from a transition-state calculation where a β electron is transferred from the HOMO to the LUMO (*cf.* (VII) and (VIII)). Due to the equivalence between the MO and VBCI triplet energies, the two VBCI parameters Δ and $h_{d\pi}$ can be determined from the two Xα transition-state energies ΔE_1 and ΔE_2. Thus, Δ is given by (*cf.* Figure 3, right)

$$\Delta = \Delta E_1 - \Delta E_2 \qquad (8)$$

and $h_{d\pi}$ results from (*cf.* (2))

$$2[(\Delta/2)^2 + h_{d\pi}{}^2]^{1/2} = \Delta E_1 + \Delta E_2 \qquad (9)$$

(18) Didziulis, S. V.; Cohen, S. L.; Gewirth, A. A.; Solomon, E. I. *J. Am. Chem. Soc.* **1988**, *110*, 250–268.

Finally, the energy of the DCT state can also be estimated with the help of Xα transition-state calculations. Starting from the triplet GS (VI), the two electrons in $(\pi^*_\sigma)'$ are moved to the HOMO and the LUMO, and the two transition energies are added.

In summary, the molecular orbital description can be used to quantitatively calculate triplet ground and CT state energies and, due to the correspondence to the VBCI formalism, thus provides values for the VBCI parameters. It further gives a physical meaning to the triplet CT state splitting ΔE_2 in Figure 3. Noting that the higher energy component $^3B_{3u}{}^{CT}$ is reached from the lower energy component $^3A_g{}^{CT}$ by a one-electron transition from the HOMO to the LUMO (*vide supra*), the triplet CT state splitting is given by the HOMO–LUMO gap:

$$\Delta E_2 \approx \Delta E_{HL} \tag{10}$$

Once all the parameters and the triplet energies are determined, the VBCI scheme (eqs 3 and 4) can be used to obtain the singlet energies (*cf.* Figure 3, middle). It is important to point out that in a strongly antiferromagnetically coupled dimer, only the singlet component of the GS is populated. Thus, only singlet GS → singlet CT transitions are likely to be observed in the absorption spectrum. The VBCI model predicts the singlet CT state splitting to be opposite that of the CT triplets (see Figure 3 and eqs 2–4) but reduced by the interaction of $^1A_g{}^{CT}$ with $^1A_g{}^{DCT}$. If $E_{DCT} \gg \Delta$, the singlet CT state splitting also reflects the absolute value of the HOMO–LUMO splitting and thus provides direct information about the bonding interaction of the bridging ligand with the metal centers. Further, both singlet CT states are shifted to lower energy by interaction with the MMCT states of equal symmetry, whereas no such interaction exists for the triplet CT states. Hence, the singlet CT are at lower energy than the triplet CT states, which corresponds to an antiferromagnetic interaction in the CT excited state (excited-state antiferromagnetism, ESAF). As a measure of ESAF, we define the energy difference between the admixed CT states (see Figure 3):

$$-2J^{CT} = \Delta E[^3B_{3u}{}^{CT} - {}^1A_g{}^{CT}] \tag{11}$$

The physical origin of this interaction is the presence of two unpaired electrons in a ligand and a metal orbital having large overlap (cf. (II)). Since the triplet ground state interacts with the triplet CT excited state and the singlet ground state with the singlet CT excited state, the antiferromagnetic interaction in the CT excited state is transferred into the ground state and, thus, is the origin for the ground-state antiferromagnetism. With the ground state–CT excited state mixing coefficient λ, the admixed singlet and triplet ground-state functions are given by

$$(^1A_g{}^{GS})' = (1-\lambda^2)^{1/2}\,{}^1A_g{}^{GS} + \lambda\,{}^1A_g{}^{CT} \tag{12}$$

$$(^3B_{3u}{}^{GS})' = (1-\lambda^2)^{1/2}\,{}^3B_{3u}{}^{GS} + \lambda\,{}^3B_{3u}{}^{CT} \tag{13}$$

Hence, GSAF as defined by the exchange constant $-2J^{GS}$ is given by

$$\begin{aligned} -2J^{GS} &\equiv \Delta E[^3B_{3u}{}^{GS} - {}^1A_g{}^{GS}] \\ &= \lambda^2 \Delta E[^3B_{3u}{}^{CT} - {}^1A_g{}^{CT}] \\ &= \lambda^2(-2J^{CT}) \end{aligned} \tag{14}$$

In summary, the VBCI description of the electron structure of bridged dimers provides a simple and spectroscopically useful model allowing the calculation of CT state energies and splittings. By comparison with the molecular orbital description of triplet CT states, the splitting of CT states can be related to the HOMO–LUMO gap ΔE_{HL} and thus provides direct experimental information about this chemically important quantity in dimers. In addition, the VBCI model allows a quantitative estimate of excited-state antiferromagnetism (ESAF) and relates its magnitude to the ground-state coupling constant $-2J^{GS}$. This ESAF is the reason for the experimental observation that bridging ligand → Cu CT transitions are at lower energy in a dimer relative to a corresponding mononuclear complex containing the same ligand and is thus the origin of "dimer" bands. As a specific application, the VBCI model is employed in the following section to interpret the peroxide → Cu(II) CT spectrum of oxyhemocyanin and to relate this to the ground-state antiferromagnetic coupling.

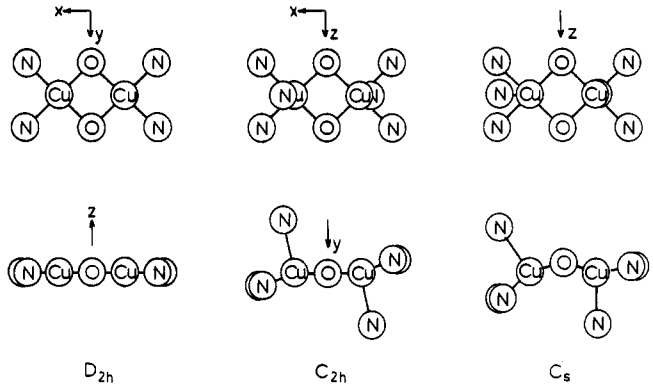

Figure 4. Coordination geometries for μ-η^2:η^2 peroxo-bridged Cu dimers from top (upper row) and side (lower row) perspectives. Coordinate systems are included. Left, planar four-coordinate (D_{2h}); middle, nonplanar five-coordinate with trans-axial ligands (C_{2h}); right, nonplanar five-coordinate with butterfly distortion (C_s). Note that the butterfly results from the trans-axial structure by bending the two Cu–O_2 planes around the O–O (z) axis.

III. Application to Oxyhemocyanin

The structure of the μ-η^2:η^2 peroxide-bridged binuclear copper complex used as a model for the active site of oxyhemocyanin is shown in Figure 4.[20] The N_3O_2 coordination around each cupric ion is approximately square pyramidal with trans-axial ligands, and the effective dimer symmetry is C_{2h}, with the $C_2 \equiv z$ axis going through the O–O vector (Figure 4, middle). However, since the bond to the apical nitrogen atom (Cu–N bond length 2.258 Å) is longer than the two other Cu–N bonds (2.000 and 1.993 Å), the apical N is initially neglected, and the copper coordination is described as square planar (N_2O_2). This increases the effective dimer symmetry to D_{2h} (Figure 4, left). With the $C_2 \equiv z$ azis perpendicular to the Cu–O_2–Cu plane and the x axis parallel to the Cu–Cu vector, the selection rules for the spin-allowed singlet $\pi^*_v(O_2^{2-}) \rightarrow$ Cu(II) LMCT transitions are $B_{2g}(R_y)$ and $B_{1u}(z)$ and for the singlet $\pi^*_\sigma(O_2^{2-})$ transitions are A_g (forbidden) and $B_{3u}(x)$. Hence, four transitions are predicted, three of which should be observable in the optical absorption (B_{1u} and B_{3u}) and CD (B_{2g}) spectra. The spectrum of oxyHc from *Busycon canaliculatum* is presented in Figure 5.[9,16] There are two intense absorption bands, one in the visible (580 nm; ϵ = 1000 M^{-1} cm^{-1}) and one in the UV (350 nm; ϵ = 20 000 M^{-1} cm^{-1}), and one CD feature at 480 nm (ΔE = +2.5 M^{-1} cm^{-1}). All these features are absent in the Met derivative when peroxide is displaced from the binuclear cupric active site and are therefore assigned as $O_2^{2-} \rightarrow$ Cu(II) charge-transfer transitions. The weak bands in the 700–800-nm region remain and are assigned as d → d transitions of tetragonal Cu(II). From overlap and energy

(19) Hay, P. J.; Thibeault, J. C.; Hoffmann, R. *J. Am. Chem. Soc.* **1975**, *97*, 4884–4899.

(20) The ligand HB(3,5-$iPr_2pz)_3$ is hydridotris(3,5-diisopropylpyrazolyl)-borate. (a) Kitajima, N.; Fujisama, K.; Moro-oka, Y.; Toriumi, K. *J. Am. Chem. Soc.* **1989**, *111*, 8975–8976. (b) Kitajima, N.; Koda, T.; Hashimoto, S.; Kitagawa, T.; Moro-oka, Y. *J. Chem. Soc., Chem. Commun.* **1988**, *110*, 3690–3692.

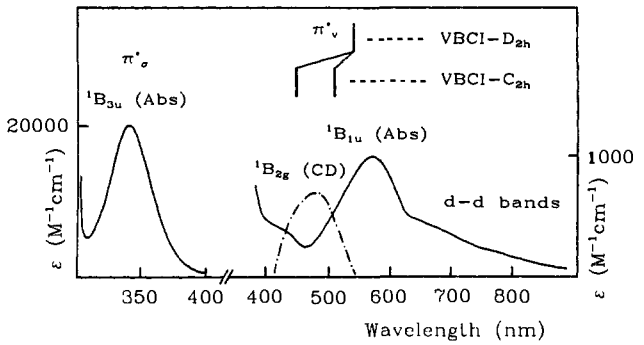

Figure 5. UV-vis absorption (solid line) and CD spectrum (broken line) of oxyhemocyanin (*Busycon*) (room temperature) along with calculated π^*_v CT transition energies in D_{2h} and C_{2h} symmetry.

considerations, the high-intensity band at 29350 cm^{-1} is assigned to the $\pi^*_\sigma \rightarrow$ Cu(II) ($^1B_{3u}$) charge-transfer transition, the low-intensity electric-dipole transition at 17 850 cm^{-1} to the $\pi^*_v \rightarrow$ Cu ($^1B_{1u}$) CT transition, and the CD feature at 21 000 cm^{-1} to the $\pi^*_v \rightarrow$ Cu ($^1B_{2g}$) CT transition (data for *Busycon* at 15 K,[16] cf. Table 1). Note that the $^1B_{2g}$ CD transition at 480 nm does not contribute to the absorption spectrum (Figure 5), as predicted by group theory. The spectrum of the side-on peroxide-bridged, binuclear cupric model complex $(Cu(HB(3,5\text{-}iPr_2pz)_3)_2(O_2)$ is very similar to that of oxyHc, and the same assignments apply,[11] i.e., the $\pi^*_\sigma \rightarrow$ Cu ($^1B_{3u}$) transition is observed at 28 600 cm^{-1} (ϵ = 26 000 M^{-1} cm^{-1}) and the $\pi^*_v \rightarrow$ Cu ($^1B_{1u}$) transition at 18 600 cm^{-1} (ϵ = 2000 M^{-1} cm^{-1}); however, no CD signal is observed due to the lack of optical activity (Table 1). These assignments are supported by the resonance Raman profiles of the O–O stretching vibration (observed at ~750 cm^{-1}) for both the side-on dimer[11] and oxyHc.[21]

The VBCI model is now applied to the $\pi^*_\sigma \rightarrow$ Cu CT transition of the side-on peroxide-bridged binuclear cupric dimer. Its electronic structure description and CT transition energies have been obtained earlier using broken-symmetry Xα calculations.[13] Now, full symmetry (D_{2h}) transition-state calculations of triplet CT excited states are required in order to obtain theoretical values for the VBCI parameters $h_{d\pi}$ and Δ (see section II). Based on the same input geometry and sphere radii as in ref 13 (Cu sphere radius 2.95 a_0), the SCF-Xα transition energy ΔE_1 from the triplet ground state ($^3B_{3u}^{GS}$) to the triplet $^3A_{1g}^{CT}\pi^*_\sigma \rightarrow$ Cu CT state is calculated to be at 62 880 cm^{-1} and the triplet CT state splitting $\Delta E_2 = \Delta E[^3B_{3u}^{CT} - {}^3A_g^{CT}]$ at 8450 cm^{-1} (Table 2). By eqs 8 and 9, these energies give a zeroth-order CT energy Δ of 54 430 cm^{-1} and a transfer integral $h_{d\pi}$ of –23 050 cm^{-1}. E_{DCT} is estimated to be at 140 000 cm^{-1}, and U is set to 6.5 eV, as described in section II. By diagonalization of the VBCI matrices 3 and 4, the energies of the two singlet $\pi^*_\sigma \rightarrow$ Cu LMCT transitions are calculated at 41 060 ($^1B_{3u}^{CT}$) and 43 780 cm^{-1} ($^1A_g^{CT}$). Compared with the experimental $^1B_{3u}^{CT}$ transition energy of 29 000 cm^{-1}, the VBCI value is over 10 000 cm^{-1} too large but represents a significant improvement over the broken-symmetry SCF-Xα result of 66 800 cm^{-1} obtained with the same Cu sphere radius. It has been shown that a reduction of the Cu sphere size results in a decrease of the Xα $\pi^*_\sigma \rightarrow$ Cu(II) CT transition energy,[13] which would also further lower the VBCI π^*_σ transition energy and thus reduce the residual discrepancy to the experimental value. The large difference between the broken-symmetry MO and the VBCI results is due to excited-state antiferromagnetism $-2J^{CT}$, which is not taken into account in the MO transition-state calculation. The VBCI model predicts a value of 29 800 for $-2J^{CT}$, i.e., the singlet $^1A_g^{CT}$ state is lowered by this amount relative to the triplet $^3B_{3u}^{CT}$ state (*cf.* eq 11). As described in section II, the excited-state antiferromagnetism is transferred into the ground state, leading to a $-2J^{GS}$ value of 2250 cm^{-1}.

The SCF-Xα transition energy from the triplet ground to the triplet $\pi^*_v \rightarrow$ Cu CT excited state is calculated in analogy to that of the π^*_σ transition by moving one electron from the π^*_v orbital to the HOMO:

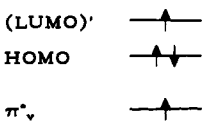

(IX)

This gives a zeroth-order π^*_v CT energy Δ_v of 7740 cm^{-1} (Table 2). Adding the depression of the $^1A_g^{GS}$ singlet ground state due to CI with the π^*_σ CT state gives a singlet $\pi^*_v \rightarrow$ Cu CT transition energy of 18 400 cm^{-1}, which compares well with the experimental result (17 000–21 000 cm^{-1}; cf. Table 2). In D_{2h} symmetry, however, no splitting is predicted by the VBCI model since the π^*_v singlet states transform as $^1B_{1u}$ and $^1B_{2g}$ and, hence, do not interact with either the ground state or the π^*_σ CT, MMCT, or DCT state. In order to account for the π^*_v state splitting observed in the electronic spectrum of oxyHc, i.e., the energy separation between the 580-nm absorption band and the CD feature at 480 nm in Figure 5, the nonplanar dimer symmetry (Figure 4, middle) has to be considered. This involves inclusion of the trans-axial ligands, which lowers the dimer symmetry to C_{2h} and results in a nonplanar structure. In C_{2h} symmetry, the peroxide π^*_v and π^*_σ orbitals both transform according to the same irreducible representation, B_g, and each $\pi^*_v \rightarrow$ Cu(II) and $\pi^*_\sigma \rightarrow$ Cu(II) CT state splits into $A_g(R_z)$ and $B_u(x,y)$ components ($z \parallel$ O–O). Due to the pyramidal coordination, the quantization axis of each copper center is now tilted with respect to the Cu–O_2–Cu plane defining π^*_σ and π^*_v (see Figure 4, middle), and there exists a nonvanishing transfer matrix element $(h_{d\pi})_v = \sqrt{2}\langle\pi^*_v|h|d_A\rangle$ between d_A, the Cu $d_{x^2-y^2}$ orbital, and π^*_v. Note that this matrix element is zero in D_{2h} symmetry due to the orthogonality of $d_A = d_{x^2-y^2}$ and π^*_v in Figure 1. In parallel, the electric dipole transition from π^*_v to d_A, which has been allowed group theoretically in D_{2h} symmetry (out of the Cu–O_2–Cu plane) but had zero intensity due to the orthogonality of π^*_v and d_A, obtains intensity in C_{2h} to the extent that the copper centers are tilted with respect to the Cu–O_2–Cu plane. We make the approximation that the electric dipole transition moments $\langle d_A|\mu|\pi^*\rangle$ are proportional to the transfer matrix elements $h_{d\pi}$, i.e.,

$$\frac{\langle d_A|\mu|\pi^*_v\rangle}{\langle d_A|\mu|\pi^*_\sigma\rangle} = \frac{(h_{d\pi})_v}{h_{d\pi}} \tag{15}$$

The oscillator strengths of the π^*_σ and $\pi^*_v \rightarrow$ Cu(II) CT transitions in Figure 5 give a ratio of 1/3.5 for eq 15 and, with $h_{d\pi}$ = –23 050 cm^{-1}, give a value of –6600 cm^{-1} for $(h_{d\pi})_v$. Note that the nonzero value of $(h_{d\pi})_v$ allows the $^1A_g(\pi^*_v)$ state to interact with the ^1A_g ground state and with the ^1A_g MMCT state, whereas $^1B_u(\pi^*_v)$ interacts only with the ^1B_u MMCT state. Further, there is no interaction between the π^*_v and the π^*_σ LMCT states, as the matrix element $\langle\pi^*_v|h|\pi^*_\sigma\rangle$ is still zero. Finally, the DCT states with two electrons removed from π^*_v or one from π^*_v and one from π^*_σ are neglected, as their energy is large as compared to the off-diagonal matrix element $(h_{d\pi})_v$. In total, one obtains the ^1A_g configurational interaction matrix 16:

	GS	CT(π^*_σ)	MMCT	DCT	CT(π^*_v)
GS	0	$h_{d\pi}$	0	0	$(h_{d\pi})_v$
CT(π^*_σ)	$h_{d\pi}$	Δ	$h_{d\pi}$	$\sqrt{2}h_{d\pi}$	0
MMCT	0	$h_{d\pi}$	U	0	$(h_{d\pi})_v$
DCT	0	$\sqrt{2}h_{d\pi}$	0	E_{DCT}	0
CT(π^*_v)	$(h_{d\pi})_v$	0	$(h_{d\pi})_v$	0	Δ_v

(16)

(21) (a) Larrabee, J. A.; Spiro, T. G. *J. Am. Chem. Soc.* **1980**, *102*, 4217–4223. (b) Freedman, T. B.; Loehr, J. S.; Loehr, T. M. *J. Am. Chem. Soc.* **1976**, *98*, 2809–2815.

Table 1. Spectroscopic Properties of Oxyhemocyanins at Room Temperature and Low Temperature[a] and of the Side-on Peroxo-Bridged Binuclear Cu(II) Model Complex $[Cu(HB(3,5\text{-}iPr_2pz)_3)]_2(O_2)$

	Busycon canaliculatum	*Limulus polyphemus*	*Cancer borealis*	model complex
$\pi^*_\sigma \rightarrow$ Cu CT (300 K) ($^1B_{3u}$)	28 850[b] (~20 000)	29 520 (~20 000)	29 850 (~20 000)	
(15 K) ($^1B_{3u}$)	29 350 (~20 000)	30 000 (~20 000)	30 350 (~20 000)	
(220 K) ($^1B_{3u}$)				28 600 (26 000)
$\pi^*_v \rightarrow$ Cu CT (300 K) ($^1B_{2g}$)	20 250 (50)[b]	20 000 (35)	19 500 (310)	
($^1B_{1u}$)	17 500 (1000)[b]	17 000 (960)	17 250 (780)	
(15 K) ($^1B_{2g}$)	21 000 (20)	20 250 (45)	20 000 (180)	
	17 850 (1180)	17 500 (1200)	18 125 (1090)	
(220 K) ($^1B_{1u}$)				18 600 (2000)
$\Delta\pi^*_v = {}^1B_{2g} - {}^1B_{1u}$ (300 K)	2750	3000	2250	
(15 K)	3150	2750	1875	
d–d bands (300 K)	13 800 (230)[b]	13 700 (300)	14 390 (520)	
(15 K)	14 280 (250)	14 280 (500)	15 000 (890)	
(220 K)				14 800 (200)
425-nm band (300 K)	23 000 (360)	23 000 (580)	23 000 (830)	
(15 K)	23 500 (400)	23 600 (890)	23 500 (1700)	

[a] At ~15 K. Energies in cm^{-1}. Absorption coefficients given in parentheses in M^{-1} cm^{-1}. [b] From Figure 5.

Table 2. Results from the SCF-Xα Transition-State Calculations,[a] VBCI Parameters Derived from These Xα Calculations,[b] and Results from VBCI Calculations[c] for Oxyhemocyanin in Planar (D_{2h}) and Nonplanar (C_{2h}) Symmetry (in cm^{-1})

	D_{2h}	C_{2h}
ΔE_1[a]	$\Delta E[^3A_g^{CT} - {}^3B_{3u}^{GS}] = 62\,880$	
ΔE_2[a]	$\Delta E[^3B_{3u}^{CT} - {}^3A_g^{CT}] = 8450$	
Δ_v[a]	$\Delta E[^3B_{2g}^{CT} - {}^3B_{3u}^{GS}] = 7740$	
Δ[b]	54 430	54 430
$h_{d\pi}$[b]	−23 050	−23 050
$(h_{d\pi})_v$[b]	0	−6600
E_{DCT}[b]	140 000	140 000
U	52 430	52 430
π^*_σ[c]	$\Delta E[^1B_{3u}^{CT} - {}^1A_g^{GS}] = 41\,060$	$\Delta E[^1B_u^{CT} - {}^1A_g^{GS}] = 44\,330$
	$\Delta E[^1A_g^{CT} - {}^1A_g^{GS}] = 43\,780$	$\Delta E[^1A_g^{CT} - {}^1A_g^{GS}] = 46\,260$
π^*_v[c]	$\Delta E[^1B_{1u}^{CT} - {}^1A_g^{GS}] = 18\,440$	$\Delta E[^1B_u^{CT} - {}^1A_g^{GS}] = 19\,520$
	$\Delta E[^1B_{2g}^{CT} - {}^1A_g^{GS}] = 18\,440$	$\Delta E[^1A_g^{CT} - {}^1A_g^{GS}] = 22\,410$
$-2J^{GS}$[c]	2250	2480
$-2J^{CT}$[c]	29 800	29 750

[a] SCF-Xα transition state calculations. [b] VBCI parameters derived from Xα calculations. [c] VBCI calculations.

and the ^1B_u interaction matrix 17

	$CT(\pi^*_\sigma)$	MMCT	$CT(\pi^*_v)$
$CT(\pi^*_\sigma)$	Δ	$h_{d\pi}$	0
MMCT	$h_{d\pi}$	U	$(h_{d\pi})_v$
$CT(\pi^*_v)$	0	$(h_{d\pi})_v$	Δ_v

(17)

Diagonalization of (16) and (17) gives the following single CT state energies (in cm^{-1}, see Table 2 and Figure 5): $^1B_u(\pi^*_v)$, 19 520; $^1A_g(\pi^*_v)$, 22 410; $^1B_u(\pi^*_\sigma)$, 44 330; $^1A_g(\pi^*_\sigma)$, 46 250 cm^{-1}. The calculated π^*_v state splitting $\Delta\pi^*_v$ of 2900 cm^{-1} is in good agreement with the values observed for oxyhemocyanins (2000–3000 cm^{-1}; *cf.* Table 1). The value of $-2J^{GS}$ for the ground-state magnetic coupling constant obtained with the VBCI model in C_{2h} symmetry is −2480 cm^{-1}. Comparison with the value of −2250 cm^{-1} obtained in D_{2h} symmetry (*vide supra*) shows that the π^*_v CT state contributes 230 cm^{-1} to $-2J$, which is 10% of the π^*_σ contribution. Thus far, only a lower limit of $-2J > 600$ cm^{-1} has been observed experimentally, and this VBCI value provides the best estimate of the GS antiferromagnetism of oxyHc.

In summary, the VBCI model combined with SCF-Xα molecular orbital calculations allows an understanding of the spectral features and the electronic structure of oxyhemocyanin. The VBCI model predicts a very strong antiferromagnetism in the π^*_σ CT excited state which lowers the observed CT energy by 25 000 cm^{-1} from the value predicted by broken-symmetry SCF-Xα transition-state calculations. In order to explain the observed splitting of the $\pi^*_v \rightarrow$ Cu LMCT transition, the small overlap between the copper $d_{x^2-y^2}$ and the peroxide π^*_v orbital in the actual nonplanar geometry has to be taken into account. The value of the relevant off-diagonal element $(h_{d\pi})_v$ is deduced experimentally from the intensity ratio of the π^*_v and π^*_σ transitions. Finally, the VBCI model predicts a value of the ground-state magnetic coupling constant $-2J^{GS}$ of 2500 cm^{-1}, which is an order of magnitude smaller than the antiferromagnetism in the π^*_σ CT excited state (ESAF). Comparison between the calculations in D_{2h} and C_{2h} symmetry shows that 90% of this value is due to ESAF in the π^*_σ state and that the π^*_v state contributes only 10% to $-2J^{GS}$.

IV. Discussion

The VBCI model presented and applied in this study to oxyhemocyanin has been shown to explain the prominent features in the absorption spectra of bridged transition-metal dimers, i.e., the low energy of the bridging ligand → metal charge-transfer transitions and the splitting of a CT transition into two states in a binuclear system. The low-energy shift of the CT transition corresponds to an antiferromagnetic interaction in the CT excited state which derives from the strong coupling of two electrons, one in a ligand and one in a metal-centered orbital due to direct orbital overlap. The VBCI model accounts for this excited-state antiferromagnetism (ESAF) in terms of configuration interaction (CI) between the LMCT and metal → metal (MMCT) and double CT (DCT) states. The splitting of a CT transition in a dimer is shown to result mainly from CI between the LMCT and the electronic ground state and is related to the HOMO–LUMO splitting due to the additional bonding in the dimeric complex.

Excited-state antiferromagnetism has a large effect on the CT spectrum and is, in fact, the origin of "dimer bands", i.e., low-energy, high-intensity transitions present only in the absorption spectrum of the binuclear bridged complex. If the dimer is strongly antiferromagnetically coupled in the ground state, only the $S = 0$ component of the ground state is populated, and the CT spectrum consists of only singlet transitions. Hence, no direct experimental determination of the magnitude of the excited-state antiferromagnetism is possible; this, however, can be estimated with the help of electronic structure calculations. CT energies obtained from SCF MO (e.g., SCF-Xα-SW) calculations include the effects of the bonding–antibonding interaction between the ligand and the metal(s) (which is larger in the dimer than in the monomer) and an additional stabilization of the ligand due to its charge donation to the second metal, which increases the effective nuclear charge on the ligand. Hence, MO theory predicts a dimer CT transition to be at much higher energy than that in the corresponding monomer. As an example, broken-symmetry SCF-Xα transition-state calculations give a value of 19 900 cm^{-1} for the $\pi^*_\sigma \rightarrow$ Cu CT energy of a mononuclear Cu(II) end-on peroxo complex and a value of 39 000 cm^{-1} for the energy of the same transition in the corresponding *trans*-μ-1,2-peroxo-bridged Cu(II) dimer.[13] However, the $\pi^*_\sigma \rightarrow$ Cu CT transition is observed at 19 900 cm^{-1} in the monomer[22a] and at 19 120 cm^{-1} in the dimer,[22b] i.e., experimentally, the CT energy does not show the increase predicted by MO calculations. The discrepancy between the theoretical and the experimental CT energy derives from the neglect of ESAF in MO theory. Here, the VBCI model is employed as a simple method to obtain a theoretical estimate of ESAF starting from a valence bond description of the bridged dimer. The VBCI parameters $h_{d\pi}$ (transfer matrix element) and Δ (zeroth-order CT energy) are obtained from Xα transition-state calculations of triplet LMCT excited states (eqs 8 and 9), and an estimate for the energy E_{DCT} is obtained from two successive transition-state calculations leading to the double CT (DCT) state. The energy of the MMCT state, U, is estimated from photoelectron spectroscopy to be at 6.5 eV. By applying this model to the $\pi^*_\sigma \rightarrow$ Cu(II) CT states in the side-on peroxide-bridged structure of oxyhemocyanin (Figure 4), one obtains an excited-state antiferromagnetic interaction $-2J^{CT} = \Delta E[^3B_{3u}{}^{CT} - {}^1A_g{}^{CT}]$ of 29 800 cm^{-1}. This is large and lowers the energy of the singlet π^*_σ transition from about 70 000 (triplet π^*_σ CT transition) to 41 060 cm^{-1} ($^1A_g{}^{CT} \rightarrow {}^1B_{3u}{}^{CT}$; *cf.* Table 2). The broken-symmetry value for the $\pi^*_\sigma \rightarrow$ Cu CT transition is 66 800 cm^{-1} with the same Cu sphere radius.[13] Although the VBCI value for the $^1A_g{}^{CT} \rightarrow {}^1B_{3u}{}^{CT}$ transition is still $\sim$10 000 cm^{-1} above the observed value of 30 000 cm^{-1}, it corresponds to a substantial reduction from the broken-symmetry Xα estimate which does not include ESAF.

Mixing between the CT excited-state and ground-state wave functions provides the mechanism for the antiferromagnetic interaction in the $\pi^*_\sigma \rightarrow$ Cu(II) CT excited state to be transferred into the ground state, scaled down by λ^2 (eq 14). Here, λ is the ground state–CT state mixing coefficient. Note that λ is a measure of covalency, i.e., the bonding interaction between the bridging ligand and the metal-centered orbitals. For $\lambda = 0.1$–0.3, $-2J^{GS}$ is predicted to be 1–10% of $-2J^{CT}$. Thus, for the side-on peroxo-bridged dimer, $-2J^{GS}$ is calculated to be -2250 cm^{-1} for the planar dimer geometry (point group D_{2h}), where only the peroxide π^*_σ orbital can interact with the metal d orbitals. This value is an order of magnitude smaller than the ESAF in the $\pi^*_\sigma \rightarrow$ Cu(II) CT state given above.

The other π^* orbital of peroxide, π^*_v, is orthogonal to the Cu $d_{x^2-y^2}$ orbitals in D_{2h} symmetry and cannot overlap with the $d_{x^2-y^2}$ orbitals. Hence, in the $\pi^*_v \rightarrow$ Cu CT excited state, there is no bonding interaction between the unpaired ligand electron and the unpaired electron on the metal, and no ESAF exists. This is the reason for the fact that $\pi^*_v \rightarrow$ Cu(II) CT transition energies of Cu peroxo dimers obtained with broken-symmetry Xα transition-state calculations have been found to be in reasonable agreement with the observed values. Thus, the $\pi^*_v \rightarrow$ Cu CT transition energy of the side-on peroxo dimer has been predicted to be at 16 000 cm^{-1} (Cu radius 2.95 Å),[13] which is in fair agreement with the experiment (17 000–21 000 cm^{-1}, *cf.* Table 1). In D_{2h} symmetry, the VBCI model gives a value of 18 400 cm^{-1} for the same transition. However, there is a small amount of overlap between the π^*_v and $d_{x^2-y^2}$ orbitals in the actual nonplanar geometry of the dimer (Figure 4, middle). This leads to a nonzero interaction of the singlet π^*_v CT with the MMCT and ground states. Experimental evidence for this interaction is provided by the presence of nonzero absorption intensity in the $\pi^*_v \rightarrow$ Cu $d_{x^2-y^2}$ CT transition and the splitting of the $\pi^*_v \rightarrow$ Cu CT transition observed in the optical and CD spectra of oxyhemocyanin. Inclusion of the π^*_v excited states in the VBCI matrix (eqs 16 and 17) reproduces the value of the π^*_v $^1B_{2g}/{}^1B_{1u}$ splitting in Figure 5 (2900 cm^{-1}) and increases the ground-state $-2J$ value to 2500 cm^{-1}, i.e., this π^*_v CT state contributes 250 cm^{-1} to $-2J^{GS}$, which corresponds to only 10% of the contribution of the π^*_σ CT state.

The above considerations can be related to the superexchange mechanism of ground-state magnetic coupling.[19,23] In the case of a binuclear Cu(II) complex with two unpaired metal electrons in orbitals d_A and d_B bridged by a ligand (I), the superexchange pathway via the ligand orbital involves two (virtual) one-electron transitions: one from π^*_σ to d_A, leading to the LMCT configuration (II), and a second from d_B to π^*_σ, leading to a MMCT configuration (III; note that the DCT configuration in (IV) also gives a small antiferromagnetic contribution). Thus, the study of CT states allows one to directly observe the intermediate states involved in the mechanism of GS antiferromagnetism. In terms of the VBCI model, each virtual one-electron transition is represented by a transfer matrix element $h_{d_A\pi} = h_{d_B\pi} = h_{d\pi}/\sqrt{2}$, leading to an interaction between initial and final states of the same symmetry. The second one-electron transition (LMCT $\rightarrow$ MMCT) leads to the energy lowering of the singlet CT excited states (ESAF), and the first transition (GS $\rightarrow$ CT) transmits this ESAF into the ground state. In the perturbation limit, the interaction matrices 2 and 4 give an excited-state antiferromagnetism (11) of

$$-2J^{CT} = h_{d\pi}{}^2\left(\frac{1}{U-\Delta} + \frac{1}{(E_{DCT}/2)-\Delta}\right) \qquad (18)$$

and a ground-state antiferromagnetism (14) of (*cf.* ref 17c)

$$-2J^{GS} = \frac{h_{d\pi}{}^4}{\Delta^2}\left(\frac{1}{U} + \frac{1}{(E_{DCT}/2)}\right) \qquad (19)$$

With $\Delta \ll U$, E_{DCT}, and $\lambda = -h_{d\pi}/\Delta$, (18) and (19) are related by

$$-2J^{GS} = \left(\frac{h_{d\pi}}{\Delta}\right)^2(-2J^{CT}) = \lambda^2(-2J^{CT}) \qquad (20)$$

which coincides with eq 14. Hence, the energy reduction of a particular π^* CT excited state directly probes the superexchange pathway via this orbital. From the large ESAF in the π^*_σ CT excited state, the superexchange pathway via the π^*_σ state is very efficient and gives the dominant contribution to $-2J^{GS}$, whereas, from the small ESAF in the π^*_v CT excited state, this pathway contributes little to $-2J^{GS}$.

(22) (a) Pate, J. E.; Cruse, R. W.; Karlin, K. D.; Solomon, E. I. *J. Am. Chem. Soc.* **1987**, *109*, 2624–2630. (b) Baldwin, M. J.; Ross, P. K.; Pate, J. E.; Tyeklár, Z.; Karlin, K. D.; Solomon, E. I. *J. Am. Chem. Soc.* **1991**, *113*, 8671–8679.

(23) Anderson, P. W. *Phys. Rev.* **1950**, *79*, 350–356.

The magnetic properties of the ground and CT excited states relate to the bonding of the side-on bridging peroxide in the dimer. The large value of ESAF exhibited by the $\pi^*_\sigma \rightarrow$ Cu(II)CT state is due to a large value of the transfer matrix element $h_{d\pi}$ and, hence, to a large amount of charge delocalization (donation) of the bridging peroxide toward the metals. This corresponds to a very strong bonding interaction between the copper $d_{x^2-y^2}$ orbitals and the peroxide π^*_σ orbital and makes the side-on less negative than the end-on bridging peroxide in Cu dimers.[13] By CI with the CT states, both the singlet and triplet ground states are stabilized by an energy corresponding to the HOMO–LUMO splitting (Figure 3) which, in the case of the side-on peroxo-bridged dimer, is calculated to be ~8500 cm^{-1}. The singlet ground state is further stabilized by a large ground-state antiferromagnetic interaction (~2500 cm^{-1}); both contributions stabilize the Cu^{II}_2–O_2 system with respect to loss of dioxygen as peroxide.

The electronic structure description obtained for the side-on peroxide-bridged model system can be used to obtain further insight into spectroscopic variations between the different oxyhemocyanin species.[16] The CD-active $^1B_{2g}$ component of the $\pi^*_v \rightarrow$ Cu CT transition in Figure 5 (D_{2h} symmetry) is still forbidden in C_{2h} symmetry ($^1A_g(\pi^*_v)$); however, the absorption intensity of this feature in fact increases along the sequence *Busycon* (mollusk, 20 M^{-1} cm^{-1}), *Limulus* (*Chelicerata* subphylum of arthropod, 45 M^{-1} cm^{-1}), and *Cancer* (*Mandibulata* subphylum of arthropod, 180 M^{-1} cm^{-1}). The intensities of the ligand field transitions also increase in the same sequence (see Table 2). These effects indicate an increasing loss of inversion symmetry of the oxyHc active site, corresponding to a geometric distortion away from effective C_{2h} symmetry, which appears to be approximately realized in mollusk hemocyanin. A transition at 425 nm also gains intensity upon going from mollusk to arthropod: the ϵ value of this band is only 400 M^{-1} cm^{-1} in *Busycon*, 890 M^{-1} cm^{-1} in *Limulus*, and 1700 M^{-1} cm^{-1} in *Cancer*. A band at approximately the same energy (460 nm, $\epsilon \approx 5000$ M^{-1} cm^{-1}) has been observed in a similar series of copper peroxo model complexes prepared by Karlin et al.[24] A butterfly structure has been inferred for these model complexes. Therefore, the 425-nm band is likely to be associated with a transition which is forbidden in C_{2h} symmetry but becomes allowed in lower symmetry. A butterfly distortion of the arthropod site would be generated by bending the two Cu–O_2 planes around the O–O axis (Figure 4, right). The resulting effective dimer symmetry is C_s, with the symmetry plane bisecting the O–O (z) axis, and all π^*_v and π^*_σ states transform as $A'(R_z,x,y)$. In particular, the forbidden $^1A_g(\pi^*_v)$ transition (C_{2h} symmetry) also gets A' character and can therefore borrow intensity from the intense π^*_σ transition. Hence, the intensity increase of the $^1A_g(\pi^*_v)$ transition observed from mollusk to arthropod is compatible with a butterfly distortion. The origin of the 425-nm band is less clear. This would appear at too low energy to be associated with histidine $\rightarrow$ tetragonal Cu(II) CT. Another possible assignment of the 425-nm band is the forbidden ^1A_g component of the π^*_σ transition. This would be compatible with the intensity increase of this feature observed in a butterfly distorted geometry; however, the VBCI model predicts the ^1A_g component to be at higher energy as compared to the $^1B_{3u}$ component of the π^*_σ CT excited state due to CI with the ground state, and a shift of the ^1A_g below the $^1B_{3u}$ π^*_σ excited state would require a larger CI contribution from the DCT state in Figure 3 or from other CT excited states, e.g., the MLCT associated with the O_2^{2-} σ^* orbital, which also participates in bonding.[13] This point requires further spectral study, prefereably on systems where it is intense, i.e., the model systems of Karlin et al.

Importantly, the distortion of the arthropod relative to the mollusk active site affects exogenous ligand binding to the site. Thus, the mollusk Hc exhibits catalase activity ($2H_2O_2 \rightarrow O_2 + 2H_2O$), while arthropod Hc does not.[16] In step b of the hemocyanin catalase cycle, O_2^{2-} is bound to the met site, generating

$$\text{deoxy}[Cu^ICu^I] + H_2O_2 + 2H^+ \rightarrow \text{met}[Cu^{II}Cu^{II}] + 2H_2O \quad \text{(a)}$$

$$\text{met}[Cu^{II}Cu^{II}] + H_2O_2 \rightarrow \text{oxy}[Cu^{II}Cu^{II}]O_2^{2-} + 2H^+ \quad \text{(b)}$$

$$\text{oxy}[Cu^{II}Cu^{II}]O_2^{2-} \rightleftarrows \text{deoxy}[Cu^ICu^I] + O_2 \quad \text{(c)}$$

$\text{oxy}[Cu^{II}Cu^{II}]O_2^{2-}$. Thus, structural changes affecting peroxide binding will also influence the catalase activity, and the lack of catalase activity in arthropod Hc may be correlated with a distorted site which limits its interaction with peroxide. This is in line with the greatly reduced azide binding constant of met arthropod as compared to met mollusk Hc.[16]

To summarize, the important features of the side-on peroxide-bridged binuclear cupric site of oxyhemocyanin are a strong delocalization of electron density toward the copper centers via the in-plane π^*_σ orbital leading to a large stabilization of the bound peroxide and a large antiferromagnetic coupling in the CT excited state. This excited-state antiferromagnetism is expressed by a large shift of the $\pi^*_\sigma \rightarrow$ Cu(II) transition to lower energy and is also the origin of a strong ground-state antiferromagnetic interaction, providing the dominant superexchange pathway for $-2J^{GS}$. In addition to the large stabilization of the dimer singlet and triplet ground states by configuration interaction with peroxide $\rightarrow$ Cu(II) CT states, the large value of ground-state antiferromagnetism further stabilizes the binuclear copper peroxo system toward loss of dioxygen. In contrast, the interaction between the metal $d_{x^2-y^2}$ and the peroxide π^*_v orbitals is weak due to the near-orthogonality of these orbitals. Hence, there is no excited-state antiferromagnetism in the π^*_v CT state, and this pathway does not contribute to $-2J^{GS}$. Thus, CT transitions can be used to probe individual pathways of ground-state superexchange. The splitting observed in the π^*_v state of oxyHc derives from the nonplanarity of the copper peroxo dimer due to the trans-axial ligands. Finally, the VBCI model can be used to estimate structural distortions in the side-on bridging structure of oxyHc from spectral changes which correlate to differences in reactivity.

Acknowledgment. E.I.S. thanks the NIH (Grant DK-31450) for support of this research. F.T. acknowledges the Deutsche Forschungsgemeinschaft (DFG) for a postdoctoral fellowship.

(24) Karlin, K. S.; Haka, M. S.; Cruse, R. W.; Meyer, G. J.; Farooq, A.; Gultneh, Y.; Hayes, J. C.; Zubieta, J. *J. Am. Chem. Soc.* **1988**, *110*, 1196–1207.